5096 *Inorg. Chem.* **2009**, *48*, 5096–5105
DOI: 10.1021/ic802234x

Inorganic Chemistry
Article

Amine, Amido, and Imido Complexes of Tantalum Supported by a Pyridine-Linked Bis(phenolate) Pincer Ligand: Ta−N π-Bonding Influences Pincer Ligand Geometry

Ian A. Tonks, Larry M. Henling, Michael W. Day, and John E. Bercaw*

Arnold and Mabel Beckman Laboratories of Chemical Synthesis, California Institute of Technology, Pasadena, California 91125

Received November 25, 2008

A series of tantalum imido and amido complexes supported by a pyridine-linked bis(phenolate) ligand has been synthesized. Characterization of these complexes via X-ray crystallography reveals both C_s and C_2 binding modes of the bis(phenolate) pyridine ligand, with complexes containing two or fewer strong π-donor interactions from ancillary ligands giving C_s symmetry, whereas three strong π-donor interactions (e.g., three amido ligands or one amido ligand and one imido ligand) give C_2-symmetric binding of the bis(phenolate)pyridine ligand. DFT calculations and molecular orbital analyses of the complexes have revealed that the preference for C_s-symmetric ligand binding is a result of tantalum−phenolate π-bonding, whereas in cases where tantalum−phenolate π-bonding is overridden by stronger Ta−N π-bonding, C_2-symmetric ligand binding is preferred, likely because conformationally this is the lowest-energy arrangement. This electronically driven change in geometry indicates that, unlike analogous metallocene systems, the bis(phenolate)pyridine pincer ligand is not a strong enough π-donor to exert dominant control over the electronic and geometric properties of the complex.

Introduction

The chemistry of the early transition metals has, to a large extent, been advanced by the use of bent metallocene frameworks. However, there has been increased interest in using well-defined, mono- and polydentate "non-metallocene" ligand sets to support a diverse range of organometallic complexes and transformations, catalysis, and small molecule activation studies.[1−13] Nonmetallocene ligand sets offer a wide variety of symmetries and donor groups; these traits are particularly desirable for developing catalysts capable of affecting new stereocontrolled reactions. These multidentate ligands have been used as both olefin polymerization catalysts and as scaffolds to study basic organometallic transformations.[14−33]

*To whom correspondence should be addressed. E-mail: bercaw@caltech.edu.

(1) (a) Britovsek, G. J. P.; Gibson, V. C.; Wass, D. F. *Angew. Chem., Int. Ed. Engl.* **1999**, *38*, 428–447. (b) Gibson, V. C.; Spitzmesser, S. K. *Chem. Rev.* **2003**, *103*, 283–315.
(2) Wolczanski, P. T. *Polyhedron* **1995**, *14*, 3335.
(3) Coates, G. W.; Hustad, P. D.; Reinartz, S. *Angew. Chem., Int. Ed. Engl.* **2002**, *41*, 2236–2257.
(4) Watson, D. A.; Chiu, M.; Bergman, R. G. *Organometallics* **2006**, *25*, 4731–4733.
(5) Anderson, L. L.; Arnold, J.; Bergman, R. G. *J. Am. Chem. Soc.* **2005**, *127*, 14542–14543.
(6) Ackermann, L.; Bergman, R. G.; Loy, R. N. *J. Am. Chem. Soc.* **2003**, *125*, 11956–11963.
(7) Rothwell, I. P. *Chem. Commun.* **1997**, 1331–1338.
(8) Wallace, K. C.; Liu, A. H.; Dewan, J. C.; Schrock, R. R. *J. Am. Chem. Soc.* **1988**, *110*, 4964–4977.
(9) Schrock, R. R. *Angew. Chem., Int. Ed. Engl.* **2006**, *45*, 3748–3759.
(10) Schrock, R. R.; Hoveyda, A. H. *Angew. Chem., Int. Ed. Engl.* **2003**, *42*, 4592–4633.
(11) Tsang, W. C. P.; Hultzsch, K. C.; Alexander, J. B.; Bonitatebus, P. J.; Schrock, R. R.; Hoveyda, A. H. *J. Am. Chem. Soc.* **2003**, *125*, 2652–2666.
(12) Schrock, R. R. *Chem. Rev.* **2002**, *102*, 145–179.
(13) Spencer, L. P.; Beddie, C.; Hall, M. B.; Fryzuk, M. D. *J. Am. Chem. Soc.* **2006**, *128*, 12531–12543.
(14) Mason, A. F.; Coates, G. W. *J. Am. Chem. Soc.* **2004**, *126*, 16326–16327.
(15) Tian, J.; Hustad, P. D.; Coates, G. W. *J. Am. Chem. Soc.* **2001**, *123*, 5134–5135.
(16) Tshuva, E. Y.; Goldberg, I.; Kol, M. *J. Am. Chem. Soc.* **2000**, *122*, 10706–10707.
(17) Tshuva, E. Y.; Goldberg, I.; Kol, M.; Goldschmidt, Z. *Organometallics* **2001**, *20*, 3017–3028.
(18) Tshuva, E. Y.; Groysman, S.; Goldberg, I.; Kol, M.; Goldschmidt, Z. *Organometallics* **2002**, *21*, 662–670.
(19) Groysman, S.; Goldberg, I.; Kol, M.; Genizi, E.; Goldschmidt, Z. *Adv. Synth. Catal.* **2005**, *347*, 409–415.
(20) Groysman, S.; Segal, S.; Goldberg, I.; Kol, M.; Goldschmidt, Z. *Inorg. Chem. Commun.* **2004**, *7*, 938–941.
(21) Groysman, S.; Goldberg, I.; Kol, M.; Genizi, E.; Goldschmidt, Z. *Organometallics* **2004**, *23*, 1880–1890.
(22) Groysman, S.; Goldberg, I.; Kol, M.; Goldschmidt, Z. *Organometallics* **2003**, *22*, 3793–3795.
(23) Groysman, S.; Segal, S.; Shamis, M.; Goldberg, I.; Kol, M.; Goldschmidt, Z.; Hayut-Salant, E. *J. Chem. Soc., Dalton Trans.* **2002**, 3425–3426.
(24) Freundlich, J. S.; Schrock, R. R.; Davis, W. M. *Organometallics* **1996**, *15*, 2777–2783.
(25) Freundlich, J. S.; Schrock, R. R.; Davis, W. M. *J. Am. Chem. Soc.* **1996**, *118*, 3643–3655.
(26) Baumann, R.; Davis, W. M.; Schrock, R. R. *J. Am. Chem. Soc.* **1997**, *119*, 3830–3831.
(27) Baumann, R.; Stumpf, R.; Davis, W. M.; Liang, L. C.; Schrock, R. R. *J. Am. Chem. Soc.* **1999**, *121*, 7822–7836.
(28) Liang, L. C.; Schrock, R. R.; Davis, W. M.; McConville, D. H. *J. Am. Chem. Soc.* **1999**, *121*, 5797–5798.
(29) Mehrkhodavandi, P.; Bonitatebus, P. J.; Schrock, R. R. *J. Am. Chem. Soc.* **2000**, *122*, 7841–7842.

Published on Web 05/07/2009

Scheme 1

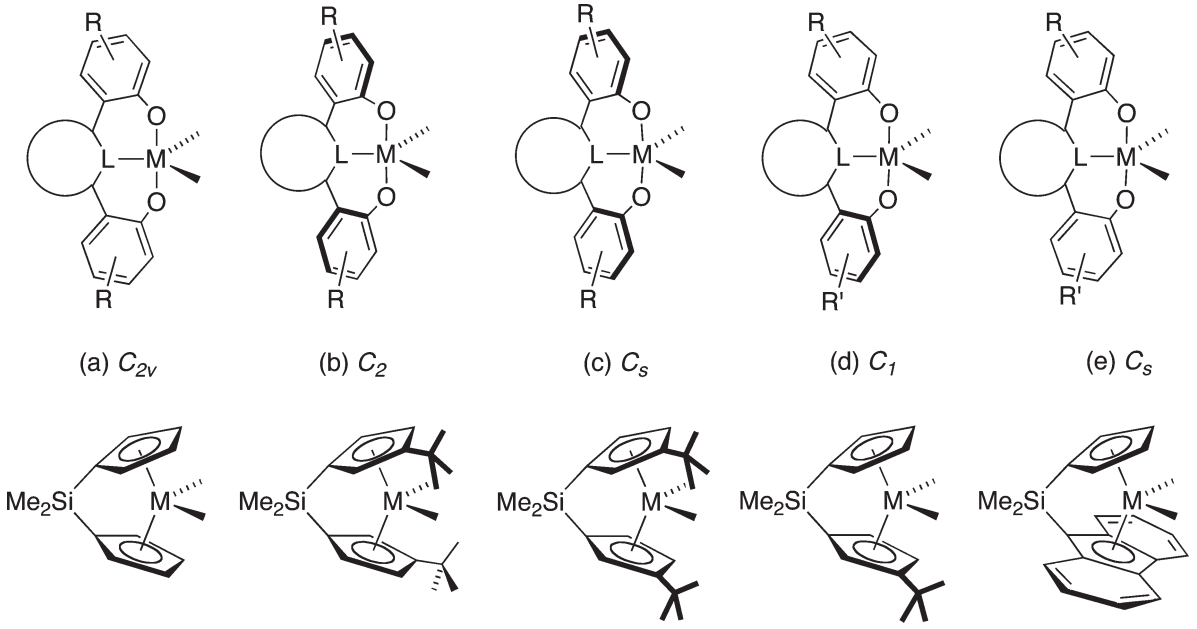

[a] R, R′ = alkyl or aryl; linker = thiophene, furan, pyrrole, pyridine, NHC, or phenyl; L = C (neutral or anionic), N, O, or S.

Recently, our group[34] and others[35,36] have been investigating the use of arene- and heterocycle-linked bis(phenolate) donor ligand sets (heterocycle = pyridine, furan, thiophene) to support titanium and zirconium polymerization catalysts[34] and as ancillary ligands for tantalum to explore other organometallic transformations.[37,38] These nonmetallocene ligand sets are connected through sp^2-sp^2 aryl−aryl, or aryl−heterocycle linkages[39] instead of more flexible sp^3-sp^3 linkages, imparting increased rigidity of the backbone, which could result in more thermally robust catalysts that are less prone to undergo ligand C−H activation.[36] One advantage of these LX_2-type ligand systems is that they easily accommodate higher oxidation states commonly found for compounds of the early transition metals. Additionally, these metal complexes with bis(phenolate)donor ligands are particularly attractive, because they have frontier orbitals similar to metallocenes[38] yet could be capable of achieving a wider range of symmetries (C_1, C_2, C_{2v}, and C_s) depending on the twist angles of the phenolate ligands (Scheme 1).[35]

With the intent to further develop the organometallic chemistry of early transition metals supported by these pincer ligands, a series of tantalum amine, amido, and imido complexes has been synthesized. These complexes have been particularly instructive for furthering our understanding of the importance of phenolate−metal π-bonding on the preferred [(ONO)Ta] symmetry and have provided insights into the differences between the [(ONO)Ta] and [Cp_2Ta] platforms. Herein, we describe the synthesis of an unusual amino−amido−imido tantalum species supported by a pyridine-linked bis(phenolate) ligand and discuss its structural preferences in relation to other new dimethylamido and phenylimido tantalum complexes having the bis(phenolate)pyridine ([(ONO)Ta]) ligand platform.

Results

Reaction of (ONO)TaMe_3 (ONO = pyridine-2,6-bis(4,6-^{t}Bu$_2$-phenolate)) with 3 equiv of aniline at 90 °C over the course of 12 h yields the imido−amido−amino tantalum complex, (ONO)Ta(NPh)(NHPh)(NH_2Ph) (**1**) (eq 1).[40] Complex **1** crystallizes from a concentrated solution of benzene upon cooling from 90 °C to room temperature and was characterized by X-ray crystallography.

(30) Mehrkhodavandi, P.; Schrock, R. R. *J. Am. Chem. Soc.* **2001**, *123*, 10746–10747.
(31) Mehrkhodavandi, P.; Schrock, R. R.; Pryor, L. L. *Organometallics* **2003**, *22*, 4569–4583.
(32) Nakayama, Y.; Saito, H.; Ueyama, N.; Nakamura, A. *Organometallics* **1999**, *18*, 3149–3158.
(33) Sernetz, F. G.; Mulhaupt, R.; Fokken, S.; Okuda, J. *Macromolecules* **1997**, *30*, 1562–1569.
(34) Agapie, T.; Henling, L. H.; DiPasquale, A. G.; Rheingold, A. L.; Bercaw, J. E. *Organometallics* **2008**, *27*, 6245–6246.
(35) (a) Chan, M. C. W.; Tam, K. H.; Zhu, N. Y.; Chiu, P.; Matsui, S. *Organometallics* **2006**, *25*, 785. (b) Chan, M. C. W.; Tam, K. H.; Pui, Y. L.; Zhu, N. Y. *J. Chem. Soc., Dalton Trans.* **2002**, 3085–3087.
(36) (a) Sarkar, S.; Abboud, K. A.; Veige, A. S. *J. Am. Chem. Soc.* **2008**, *130*, 16128–16129. (b) Sarkar, S.; Carlson, A. R.; Veige, M. K.; Falkowski, J. M.; Abboud, K. A.; Veige, A. S. *J. Am. Chem. Soc.* **2008**, *130*, 1116–1117.
(37) Agapie, T.; Bercaw, J. E. *Organometallics* **2007**, *26*, 2957–2959.
(38) Agapie, T.; Day, M. W.; Bercaw, J. E. *Organometallics* **2008**, *27*, 6123–6142.
(39) Steinhauser, S.; Heinz, U.; Sander, J.; Hegetschweiler, K. Z. *Anorg. Allg.Chem.* **2004**, *630*, 1829–1838.

(40) In all of the schemes in this paper, amido (LX) ligands will be represented as double bonds and imido ligands (LX_2) as triple bonds since these representations most accurately describe the bonding within these systems (as evidenced by simple electron counting and DFT calculations), despite this notation not being the normal convention. Additionally, all Ta−O bonds will be drawn as single bonds, although some of the Ta−O bonds in these complexes are best described as having three-center−four-electron bonds and bond orders greater than 1. See Table 1 for a full description of the Ta−O bond order in all of these complexes.

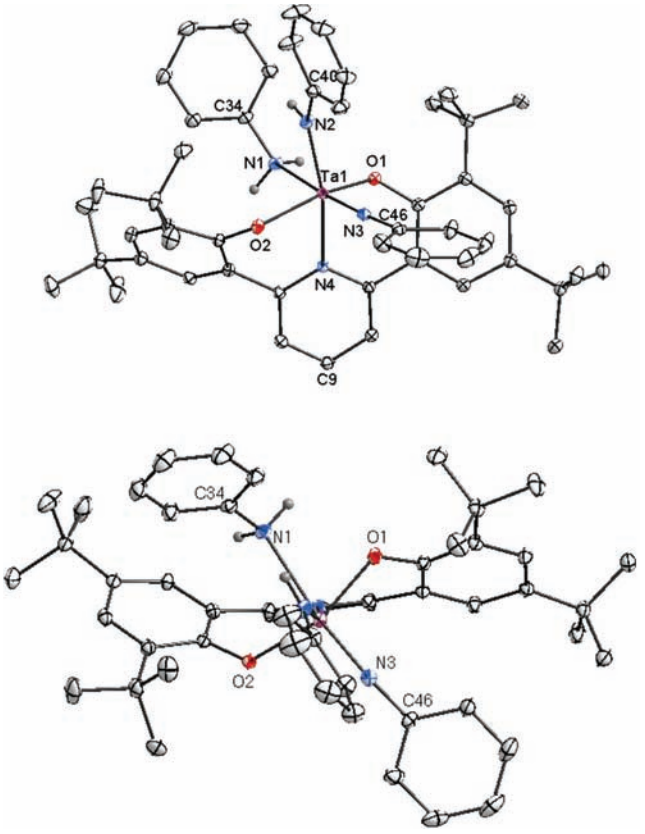

Figure 1. Thermal ellipsoid drawing of **1**. Side view and top-down view showing C_2 symmetric bisphenolate ligand. Selected bond lengths (Å) and angles (deg): Ta−O1, 2.0045(10); Ta−O2, 1.9999(11); Ta−N1, 2.4796 (13); Ta−N2, 2.0271(11); Ta−N3, 1.7865(13); Ta−N4, 2.3126(10); Ta−N4−C34, 127.21(9); Ta−N2−C40, 139.07(10); Ta−N3−C46, 176.07(11). N-bound hydrogens in calculated positions; all others omitted for clarity.

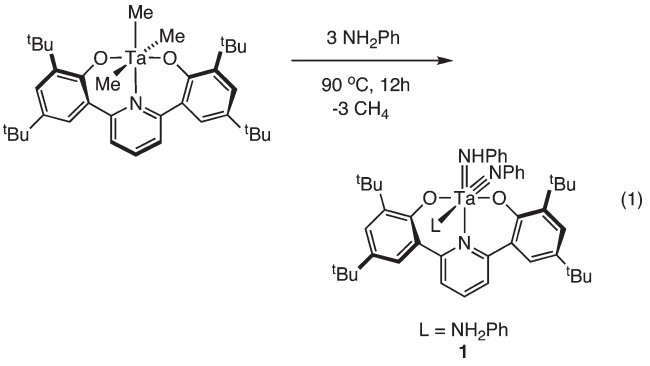

(1)

The Ta−N bond lengths for **1** (Figure 1) are indicative of three types of Ta−N bonding: 2.480(1) Å for the L-type aniline, 2.027(1) Å for the LX-type anilide, and 1.786(1) Å for the LX_2-type phenylimide. The bis(phenolate)pyridine ligand binds in a meridonal fashion, with the anilide ligand trans to the pyridine linker and aligned perpendicular to the O−Ta−O plane—opposite alignment to what was observed in the benzylidene complex (ONO)Ta(CHPh)(Bn)(PR_3).[38] This meridional binding mode is typical for early metal complexes of the bis(phenolate)pyridine ligand; however, it is the first six-coordinate tantalum complex to exhibit a C_2-symmetric binding of the ligand instead of the typically observed C_s-symmetric binding, as, for example, for the trimethyl tantalum starting material in eq 1. The dihedral angle of 58.7° between the two phenolate groups indicates a significant C_2 twist of the ligand. Additionally, the pyridine linker of **1** binds in a much more linear fashion: the Ta1−N4−C9 angle is 170.8°, whereas in the C_s-symmetric cases the angle is typically 150−160°. Interestingly, the NH protons on the L-type aniline appear as a broad singlet in the ^{1}H NMR despite being diastereotopic. We believe this is a result of equilibration due to rapid interconversion of enantiomers of the C_2 geometry in solution, probably progressing through a C_{2v}-symmetric intermediate. The average Ta−O bond distance in **1** is 2.002(1) Å, which is significantly (~0.1 Å) longer than the distances observed earlier.[38] These structural features prompted further investigation of the underlying reasons for a preference for C_2 versus C_s ligand geometry and the preferences for the ligand trans to the pyridine in these complexes.

A distinctive feature of **1** (an (ONO)Ta(L)(LX)(LX_2)-type complex), as opposed to all previously studied (ONO)TaX_3 complexes, is the presence of three strong Ta−X π bonds, one for the amido and two for the imido ligand. We therefore hypothesized that these Ta−N π bonds were responsible for the observed C_2 rather than C_s ligand geometry. A series of [(ONO)Ta] amides and imides with varying X-type, LX-type, and LX_2-type ligands, and hence differing numbers of Ta−N π bonds, were synthesized (eq 2−4).

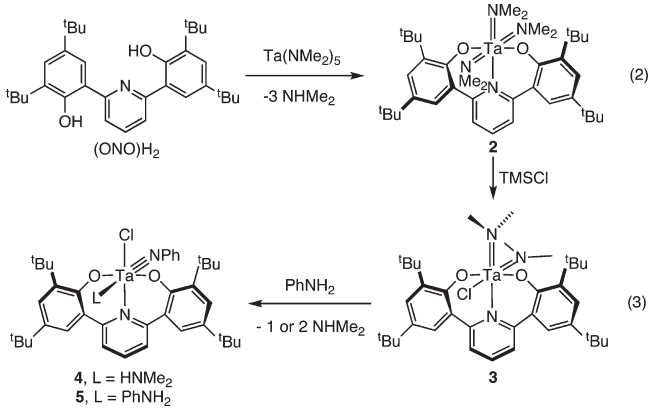

(2)

(3)

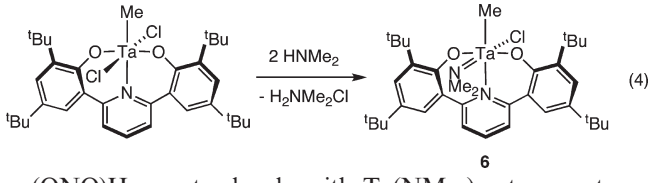

(4)

$(ONO)H_2$ reacts cleanly with $Ta(NMe_2)_5$ at room temperature in benzene to yield the tris(amide) complex (ONO)$Ta(NMe_2)_3$ (**2**). The ^{1}HNMR spectrum of **2** shows two sharp singlets at 2.975 and 3.741 ppm in a 12:6 ratio, indicative of two distinctive types of dimethylamido groups—one type cis to pyridine and the other trans, respectively. In contrast to the trimethyl complex[38] (ONO)$TaMe_3$, **2** shows no fluxional exchange between the dimethylamido groups even at elevated temperatures, likely a result of the increased preference for octahedral rather than trigonal prismatic geometry (the proposed intermediate for ligand site exchange),[38] resulting from strong Ta=N π-bonding. X-ray-quality crystals of **2** were grown from a saturated diethyl ether solution cooled to −30 °C. The crystal structure (Figure 2) of **2** reveals that the bis(phenolate)pyridine ligand binds to tantalum meridionally in a C_2-symmetric fashion, as expected for a complex

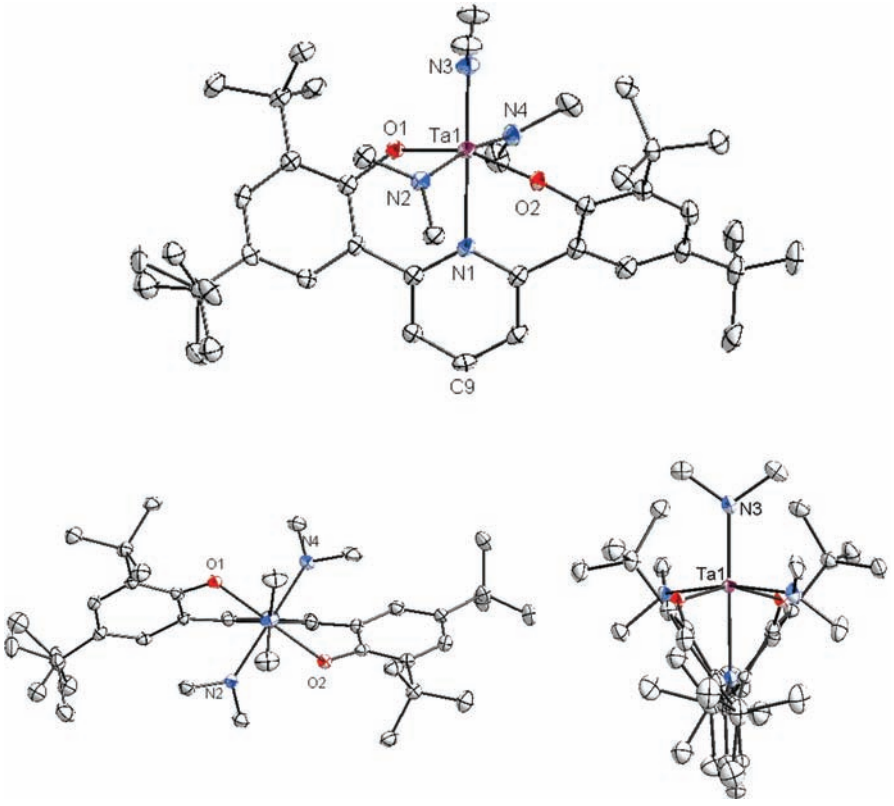

Figure 2. Thermal ellipsoid drawing of **2**. Front view, top-down view showing C_2 symmetry, and side-on view showing the bis(phenolate)pyridine dihedral angle. Selected bond lengths (Å) and angles (deg): Ta1−O1, 1.9908(18); Ta1−O2, 1.9788(18); Ta−N1, 2.3111(23); Ta1−N2, 2.0325(18); Ta1−N3, 1.9941 (24); Ta1−N4, 2.0289(18); Ta1−N1−C9, 178. H atoms admitted for clarity.

with three strong Ta−N π bonds, similar to complex **1**. In fact, the bis(phenolate)pyridine ligand in **2** shares all of the new characteristic properties observed for **1**. The dihedral angle between the two phenyl rings of the bis(phenoxide) ligand is 59.7°, again indicating a significant C_2 twist of the ligand. The Ta1−N1−C9 angle is 178°, indicating an almost linear binding of the pyridine linker, and finally, the average Ta−O bond distances are long at 1.985(2) Å. The Ta−N bond lengths of the amides cis to pyridine are slightly longer than that for the amide trans to pyridine, 2.029(2) and 2.032 (2) versus 1.994(2)Å, respectively, indicative of a slightly larger amide trans influence, but well within the range of Ta−N double bonds.

When complex **2** is treated with 1 equiv of TMSCl in benzene, the monochlorinated product (ONO)Ta$(NMe_2)_2$Cl (**3**) is generated quantitatively over the course of four days at room temperature, or in 2 h at 90 °C (see Figure 3). Complex **3** exhibits sharp singlets at 3.029 and 3.919 ppm corresponding to the dimethylamido groups cis and trans to pyridine, respectively, and similar to complex **2**, no fluxionality is observed even at elevated temperatures. X-ray-quality crystals of **3** were grown by slow evaporation from a saturated diethyl ether solution. The bis(phenolate)pyridine ligand in complex **3** binds meridionally, as for **1** and **2**, but in a C_s-symmetric fashion where the mirror plane in the molecule bisects the phenolate−tantalum−phenolate angle. One of the dimethylamides lies cis to the pyridine, while the other is trans, consistent with ^{1}H NMR, and their bond lengths are 1.979(2) Å and 1.982(2) Å, respectively—again, consistent with Ta=N double bonds. The average Ta−O phenolate bond distances in **3** are 1.924(3) Å, significantly shorter than seen in **1** and **2** (2.002(1) and 1.985(2) Å, respectively), implicating a greater degree of phenolate π-bonding in this complex. Indeed, this is expected, as one phenolate π bond is required to complete an 18-electron count at tantalum.

Reaction of 1 equiv of aniline with **3** in benzene at 90 °C for one week quantitatively yields the phenylimide chloride, (ONO)Ta(NPh)$(HNMe_2)$Cl (**4**). A similar reaction with excess aniline yields (ONO)Ta(NPh)(H_2NPh)Cl (**5**), although only limited crystallographic identification of **5** has been obtained due to twinned, unstable crystals. X-ray-quality crystals of **4** were grown by slow evaporation of a saturated benzene solution. Complex **4**, as for **3**, has a C_s-symmetric, meridionally bound bis(phenolate)pyridine ligand (Figure 4). It is interesting to note that one of the phenolate arms is twisted 13.3° away from perfect C_s symmetry, possibly due to crystal packing forces. The pyridine linker is canted out of the O−Ta−O plane by 23.3°, which is typical in the C_s-symmetric binding mode. The Ta−N distance of 1.791(3) Å is typical for tantalum imides, and the Ta1−N3−C36 angle of 174.2° indicates that it is an LX_2-type donor. The average Ta−O bond distance of 1.954(2) Å is again shorter than observed in complexes **1** and **2** and more comparable to those in complex **3**, indicating some degree of Ta−O multiple-bond character.

Reaction of an excess of $HNMe_2$ with (ONO)$TaCl_2$Me in benzene rapidly forms the mono(dimethylamido) complex, (ONO)Ta(NMe_2)MeCl (**6**), along with the concomitant precipitation of H_2NMe_2Cl. X-ray-quality crystals were obtained by cooling a saturated solution of **6** in diethylether to −30 °C overnight. Complex **6** (Figure 5) displays the usual meridonal binding of the bis(phenolate)pyridine ligand and, like complexes **3**−**5**, is C_s-symmetric. The Ta−O average bond length is 1.887(2), and the Ta−N distance of 1.975(2)

for dimethylamide is typical of a Ta=N double bond. Interestingly, the π-bonding amide in **6** lies cis to the pyridine linker, whereas in the previously reported benzylidene[38] the π-bond lies trans to pyridine. The ^{1}H NMR spectrum is consistent with a cis amide as well, as the dimethylamide singlet resonates at 3.214 ppm, in the range of the cis dimethylamide peaks seen in complexes **2** and **3**. Because a tantalum dπ orbital (d_{yz}, vide infra) is available in both cis and trans positions (vide infra), there does not appear to be a strong electronic preference. Thus, we attribute this cis preference of the amide to steric interactions for the alternate geometry; the bulkiest ligand (NMe_2) would be best accommodated in one of the cis positions. In the benzylidene example, the π-bonding benzylidene is the *least* bulky substituent. This could also be a result of the strongest trans-influencing ligand (Me or Bn) preferring to be trans to the weak pyridine ligand.

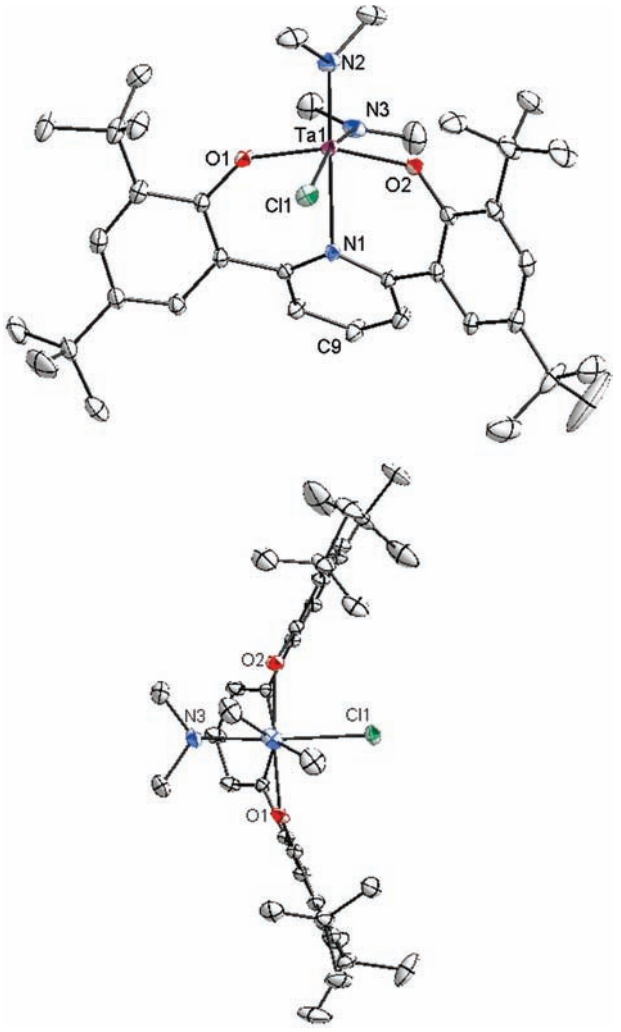

Figure 3. Thermal ellipsoid drawing of **3**. Front view (left) and top-down view (right) showing the C_s symmetry of the bis(phenolate)pyridine ligand. Selected bond lengths (Å) and angles (deg): Ta1−O1, 1.9282(15); Ta1−O2, 1.9207(17); Ta−N1, 2.3922(18); Ta1−N2, 1.9708(22); Ta1−N3, 1.9848(21); Ta1−Cl1, 2.4686(6); Ta−N1−C9, 147.78(2). H atoms omitted for clarity.

Discussion

From the structural data for complexes **1**, **2**, **3**, **4**, and **6**, as well as for other previously reported tantalum complexes having the bis(phenolate)pyridine ancillary ligand, it is apparent that the number of strong tantalum−nitrogen π bonds for the remaining three ligands significantly affects the degree of Ta−O π-bonding for two phenolates. The amount of Ta−O π-bonding can be quantified by examining the distances in the solid-state structures (Table 1). In complexes where there is no π-bonding, that is, the remaining three ligands are X-type, the average Ta−O bond length is roughly 1.9 Å. As the number of π-bonding ligands is increased, a corresponding increase in the Ta−O bond length is also observed, reaching as high as 2.0 Å in cases where there are three strong π-donating ancillary ligands, as for example is the case with **1** (L, LX, and LX_2 ligands) and **2** (three LX ligands). Thus, it is apparent that the Ta−O bond order decreases as additional strong π-bonders are introduced into the system—going from a Ta−O bond order of 2 in the case of zero π-donating ligands down to an order of 1 when there are three strong π-donating ligands. The rather small change in the Ta−O bond length over all of the compounds (~0.1 Å) is likely due to the generally poor π-donating ability of electronegative oxygen and the inherent rigidity of the system, which should limit the overall change in bond lengths.

From a molecular orbital perspective, a C_s-symmetric bis(phenolate)pyridine ligand should be able to π-bond to the metal center using lone pairs on each oxygen, making bonds

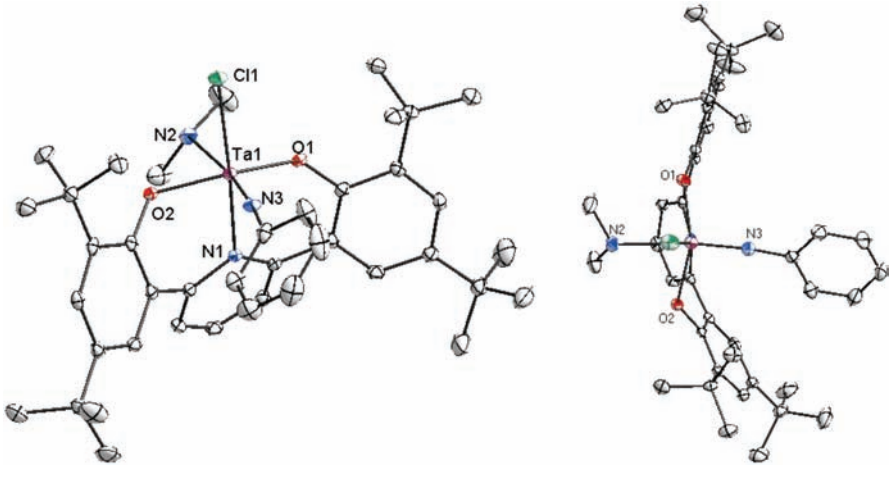

Figure 4. Thermal ellipsoid drawing of **4**. Front view (left) and top-down view (right) showing the C_s geometry of the bis(phenolate)pyridine ligand. Selected bond lengths (Å) and angles (deg): Ta1−O1, 1.9437(14); Ta1−O2, 1.9643(13); Ta−N1, 2.2918(17); Ta1−N2, 2.4568(17); Ta1−N3, 1.7841(14); Ta1−Cl1, 2.3920(5); Ta−N1−C9, 156.82(8) Ta−N3−C36, 174.2(2). H atoms removed for clarity.

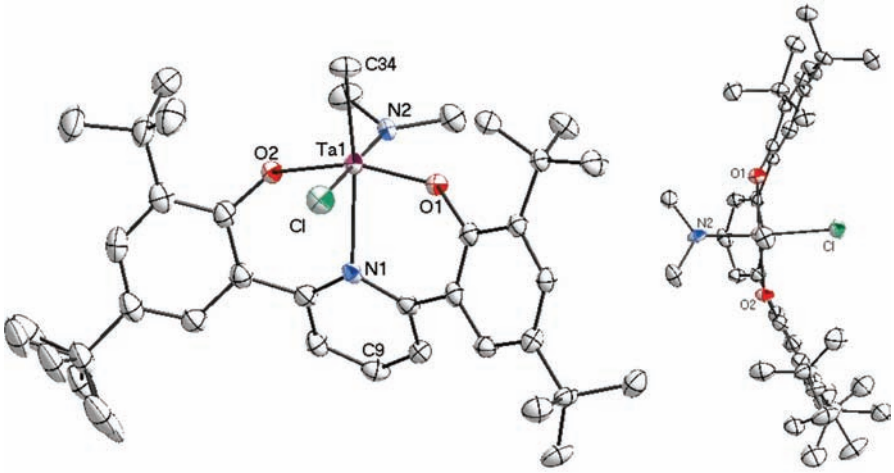

Figure 5. Thermal ellipsoid drawing of **6**. Front view (left) and top-down view (right) showing C_s symmetric binding of the bis(phenolate)pyridine ligand. Selected bond lengths (Å) and angles (deg): Ta1−O1, 1.8936(25); Ta1−O2, 1.8810(26); Ta−N1, 2.3916(31); Ta1−N2, 1.9746(37); Ta1−C34, 2.1908(51); Ta1−Cl1, 2.4683(11); Ta−N1−C9, 149.6(2). H atoms removed for clarity.

Table 1. Observed Solid State Ligand Symmetries and Average Ta-O Bond Length in Selected Tantalum (Bis)phenolate Complexes

L_3 for (ONO)TaL_3	symmetry	# of Ta=L π bonds	average TaO bond order[a]	d(TaO)$_{ave}$ (Å)
(NPh)(NHPh)(NH_2Ph) (**1**)	C_2	3	1	2.002(1)
$(NMe_2)_3$ (**2**)	C_2	3	1	1.985(2)
$(NMe_2)_2$Cl (**3**)	C_s	2	1.5	1.924(3)
(NPh)(HNMe_2) Cl (**4**)	C_s	2	1.5	1.954(2)
(NPh)(NH_2Ph) Cl (**5**)	C_s	2	1.5	1.948(3)[b]
(NMe_2)(CH_3)Cl (**6**)	C_s	1	2	1.887(2)
(=CHPh)(CH_2Ph)(PR_3)[c]	C_s	1	2	1.922(1)
$(CH_3)_3$[b]	C_s	0	2[d]	1.906(1)

[a] To complete the 18-electron count at Ta. [b] Complex not anisotropically refined. [c] Taken from ref 38. [d] A 16-electron maximum.

with d_{xz} and d_{xy} on tantalum (the bonding linear combination of oxygen p_z's (and p_y's) and tantalum d_{xz} (and d_{xy}) are shown at the top of Scheme 2). In the case of the mono (amide) **6** and the previously reported benzylidene complex,[38] where there exists only one ancillary ligand π bond, these Ta−O π interactions force the amide (or benzylidene) ligand to π-bond with d_{yz}, despite the steric consequence of forcing the amide methyls or phenyl of the benzylidene toward a phenolate *tert*-butyl group(s). However, in the case where there are two ligand π bonds such as the bis(amide) **3** or the phenylimide-chlorides **4** and **5**, one of the two Ta−O π bonds must be sacrificed to make the second ancillary ligand π-bond. For **4** and **5** (shown in Scheme 2), the remaining Ta−O π interaction occurs through d_{xz}; for **3** (not shown), interaction occurs with d_{xy}.[41] Finally, in the case where there are three strong ancillary ligand π bonds, all Ta−O π-bonding is precluded to accommodate the other ligands. In these cases, the bis(phenolate) ligand twists from C_s symmetry to C_2 symmetry. This symmetry switch is likely due to two factors. First, twisting to C_2 symmetry reduces overlap between the oxygen p orbitals and the filled N-to-Ta π bonds, reducing energetically unfavorable filled−filled repulsions. Second, this twist could be a geometric relaxation effect; the C_2 symmetry can better accommodate the large tantalum atom because twisting lengthens its Ta−O bonds. As evidenced by the canted pyridine rings, C_s symmetry, while increasing Ta−O bonding, also forces an unnatural Ta−pyridine bond length. The implication of either explanation is that any oxygen π-bonding encourages C_s-symmetric binding, since the overlap between the tantalum d orbitals and occupied oxygen p orbitals is essentially lost in the C_2 geometry.

DFT calculations (B3LYP, 6-31G**, LANL2DZ Ta pseudopotential) were performed on complex **1** in order to affirm the bonding description described above. A structural optimization starting from the crystal structure coordinates was performed and produced a structure very similar to the experimentally observed one. The calculated HOMO, HOMO-1, and HOMO-2 distinctly show the anilide-d_{xz}, imide-d_{yz}, and imide-d_{xy} π-bonding interactions, consistent with the bond distances observed in the crystal structure (Figure 6). Notably absent in the calculated results is any phenolate−tantalum three-center−four-electron π-bonding, which is observed in other calculations performed on complexes supported by this ligand set.[38] The absence of phenolate π-bonding is, however, not entirely surprising; assuming that the phenylimide and anilide are stronger π donors than the phenolate, no phenolate π-bonding would be necessary to complete the 18-electron count at tanatalum. This bonding picture, however, is very different from its earlier-reported metallocene counterpart Cp^*_2Ta(=NPh)(H).[42] In the metallocene case, rather than displace the strong Cp^*−Ta bonds, the nitrogen lone pair remains nonbonding—demonstrating one key difference between the bis(phenolate)pyridine and metallocene ligand systems: unlike metallocenes, phenolates are not strong enough π donors to effectively compete with strong π-donating ancillary ligands such as imido and amido.

In order to address the possibility of steric repulsion driving the C_s-to-C_2 geometry switch, DFT calculations

(41) One might question why the imido ligand of complexes **4** and **5** does not occupy the site trans to pyridine in order to preserve the phenolate-to-d_{xy} π-bonding. We do not fully understand the preference for a cis imido, but the weakest trans influencing L-type amine ligand may direct the imido.

(42) Parkin, G.; van Asselt, A.; Leahy, D. J.; Whinnery, L.; Hua, N. G.; Quan, R. W.; Henling, L. M.; Schaefer, W. P.; Santarsiero, B. D.; Bercaw, J. E. *Inorg. Chem.* **1992**, *31*, 82–85.

(B3LYP, 6-31G**, LANL2DZ Ta pseudopotential) were also carried out on simpler complexes with significantly less steric bulk than the synthesized complexes. In all of these cases, the ortho and para *tert*-butyl groups in the ligand backbone were removed. Calculations were performed on $(ONO)Ta(NH_3)(NH_2)(NH)$ and $(ONO)Ta(NMe_2)_3$, which are expected to be C_2-symmetric according to the bonding arguments above. The expected C_2 symmetry is obtained upon optimization of both C_{2v} and C_2 unoptimized starting structures. Similarly, calculations on $(ONO)Ta(NH_2)_2Cl$, $(ONO)Ta(NH_3)(NH)Cl$, and $(ONO)Ta(NMe_2)_2Cl$, expected to display C_s symmetry, also yielded this symmetry upon optimization from either C_{2v} or C_s unoptimized starting structures. The optimized structures from these calculations are shown in Figure 7. It is noteworthy that, in $(ONO)Ta(NMe_2)_3$ and $(ONO)Ta(NMe_2)_2Cl$, which differ from their synthesized analogues only by removal of the *tert*-butyl bulk, the optimized structures do not significantly (<0.01 Å Ta−O bond length and $<0.7°$ phenolate torsion angle) differ from the structures obtained from X-ray diffraction. Additionally, small steric effects can be seen by comparing the optimized structures of $(ONO)Ta(NH_2)_2Cl$ and $(ONO)Ta(NMe_2)_2Cl$. In the case of $(ONO)Ta(NH_2)_2Cl$, the NH_2 trans to pyridine lies perpendicular to the O−Ta−O plane, while in $(ONO)Ta(NMe_2)_2Cl$, the dimethylamide is twisted away from perpendicular. We attribute this twist to a small steric effect which is also seen in complexes **2** and **3**; it is notable that, while the amide ligands rotate to reduce steric repulsion, no perturbation of

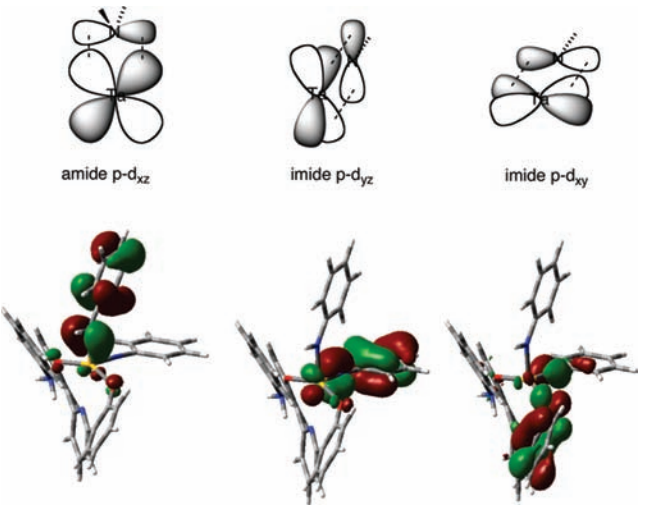

Figure 6. DFT calculations (B3LYP, 6-31G**, LANL2DZ Ta pseudopotential) showing HOMO, HOMO-1, and HOMO-2 (L-R), representing the three Ta−N π bonds in complex **1**.

Scheme 2

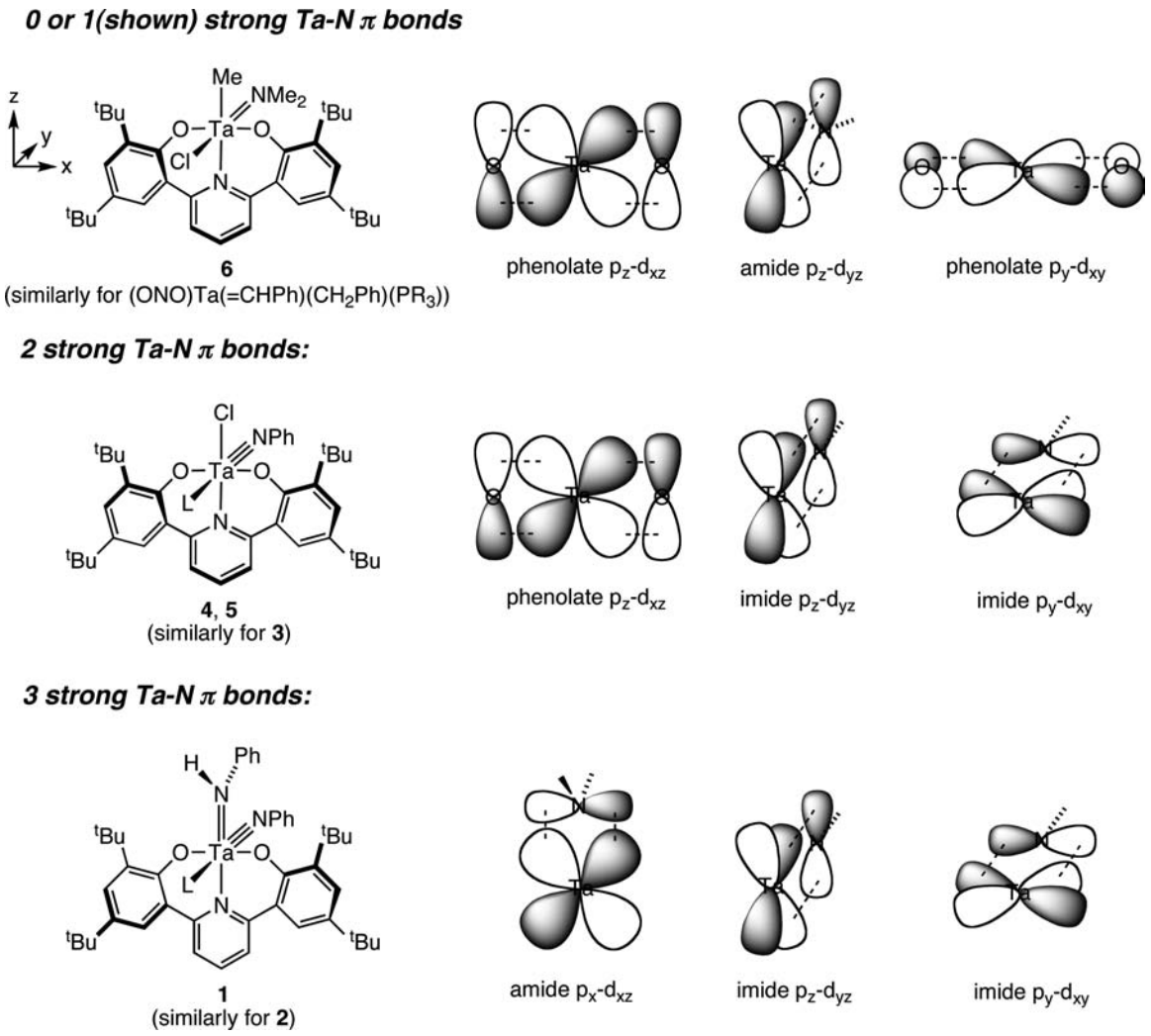

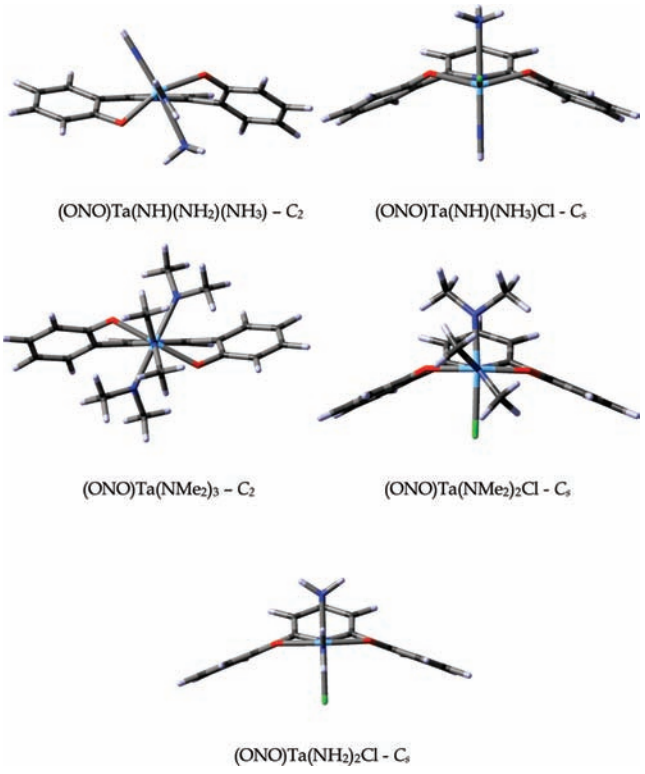

Figure 7. DFT (B3LYP, 6-31G**, LANL2DZ Ta pseudopotential) optimized structures (see text) of calculated complexes displaying C_2- and C_s-symmetric structures with significantly smaller ligands.

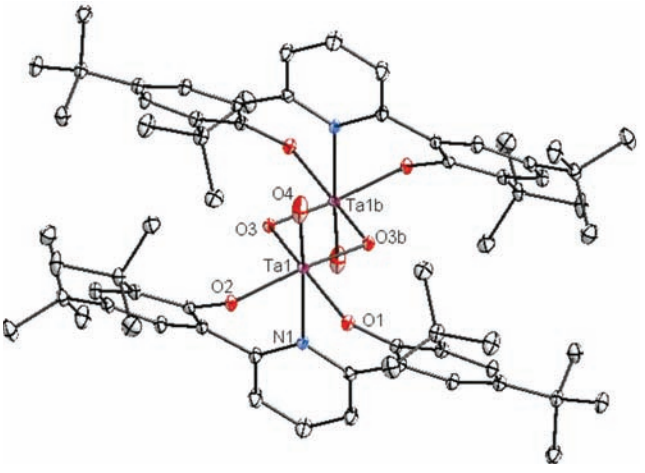

Figure 8. Thermal ellipsoid drawing of **7**. Front view showing fac-binding of the bis(phenolate)pyridine ligand. Selected bond lengths (Å): Ta1−O1, 1.9502(5); Ta1−O2, 1.9622(5); Ta−O3, 1.9431(5); Ta1−O3b, 1.9328(5); Ta1−O4, 2.0733(8); Ta1−N1, 2.3120(5); Ta1−Ta1b, 2.9917 (1). H atoms removed for clarity.

the (ONO) framework is observed. These results, as well as earlier observations that other quite bulky complexes based on this ligand set such as (ONO)Ta(Bn)(CHPh)(PMe_2Ph) still exhibit C_s symmetry,[38] lead us to believe that, at least when examining similar series of compounds, the steric demands of the ligands are not a major cause of geometric rearrangement.

Attempts to make the analogous tantalum oxo series of compounds have been unsuccessful to date. Instead, the reaction of (ONO)$TaMe_3$ with degassed H_2O yields oxo-bridged dimer products (eq 5).

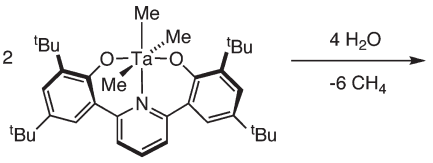

$[(ONO)Ta(OH)]_2(\mu_2\text{-}O)_2$ (+ other μ-oxo dimers) (5)

7

The bis-μ-oxo complex **7** represents the first crystallographically characterized tantalum bis(phenolate)pyridine complex that exhibits a facial binding of the ligand (Figure 8). This complex, along with a related titanium complex,[43] supports the proposed intermediacy of a facially bound isomer in the exchange of methyl groups in (ONO)$TaMe_3$, as proposed earlier.[38]

Conclusions

A series of imido and amido complexes supported by a pyridine-linked bis(phenolate) ligand have been synthesized and structurally characterized via NMR and X-ray crystallography. These complexes exhibit either a C_s- or C_2-symmetric meridional binding of the bis(phenolate) ligand. The preferred geometry appears to be determined by the degree of Ta−O π-bonding in the phenolate ligands. When Ta−O π bonds are required to complete the 18-electron count, the bis(phenolate)pyridine ligand binds in a C_s-symmetric fashion. In cases where strong π donation from ancillary ligands precludes Ta−O π-bonding (that is, when there are three strong π-donor interactions from the other ligands), the bis(phenolate) ligand twists in a C_2 fashion to reduce filled−filled repulsions between the Ta−X π bonds and the oxygen lone pairs and leads to a less strained (ONO) geometry. This electronically driven change in geometry indicates that, unlike analogous metallocene systems, the bis(phenolate) pincer ligand is not a strong enough π donor to exert total control over the electronic and geometric properties of the complex.

Experimental Section

General Considerations and Instrumentation. All air- and moisture-sensitive compounds were manipulated using standard high-vacuum and Schlenk techniques or were manipulated in a glovebox under a nitrogen atmosphere. Solvents for air- and moisture-sensitive reactions were dried over sodium benzophenone ketyl and stored over titanocene, where compatible, or dried by the method of Grubbs et al.[44] Benzene-d_6 and toluene-d_8 were purchased from Cambridge Isotopes and dried over sodium benzophenone ketyl, while methylene chloride-d_2, also purchased from Cambridge Isotopes, was dried over CaH_2 and filtered through a plug of activated alumina. $TaCl_5$ purchased from Strem Chemicals was sublimed prior to use. Amines were purchased from Sigma-Aldrich and were distilled from CaH_2 and degassed prior to use. All other materials were used as received. ^1H and ^{13}C spectra were recorded on Varian Mercury 300 or Varian INOVA 500 spectrometers, and chemical shifts are reported with respect to residual protio-solvent impurity for ^1H (s, 7.16 ppm for C_6D_5H; t, 5.32 ppm for $CDHCl_2$) and solvent carbons for ^{13}C (t, 128.39 for C_6H_6; s, 20.40 for CD_2Cl_2). 2,6-$(HOC_6H_2\text{-}{}^t Bu_2)_2C_5H_3N$, 2,6-$(OC_6H_2\text{-}{}^t Bu_2)_2C_5H_3N$)

(43) Golisz, S.; Bercaw, J. Unpublished results.
(44) Pangborn, A. B.; Giardello, M. A.; Grubbs, R. H.; Rosen, R. K.; Timmers, F. J. *Organometallics* **1996**, *15*, 1518.

$TaMe_3$, and (2,6-$(OC_6H_2$-$^tBu_2)_2C_5H_3N)TaCl_2Me$ were prepared as previously reported.[38] Despite repeated attempts, acceptable elemental analyses for complexes **1**, **4**, and **5** were not obtained, likely a result of the labile L donors or the loss of some solvent from the crystal lattices.

Computational Details. Density functional calculations were carried out using Gaussian 03, revision D.01.[45] Calculations on the model systems (with minimal steric bulk) were performed using the nonlocal exchange correction by Becke[46,47] and nonlocal correlation corrections by Perdew,[48] as implemented using the b3lyp[49,50] keyword in Gaussian. The following basis sets were used: LANL2DZ[51−53] for Ta atoms and 6-31G** basis set for all other atoms. Pseudopotentials were utilized for Ta atoms using the LANL2DZ ECP. All optimized structures were verified using frequency calculations and did not contain any imaginary frequencies. Iso-surface plots were made using the Gaussian 03, revision D.01 program.[45]

(2,6-$(OC_6H_2$-$^tBu_2)_2C_5H_3N)Ta(NPh)(NHPh)(NH_2Ph)$ (1). In an inert atmosphere glovebox, a 25 mL Schlenk flask fitted with a Teflon screwcap valve was charged with (2,6-$(OC_6H_2$-$^tBu_2)_2C_5H_3N)TaMe_3$ (100 mg, 0.141 mmol, 1 equiv) and 10 mL of C_6H_6. $PhNH_2$ (38.5 μL, 0.4225 mmol, 3 equiv) was syringed in, and the vessel was sealed and placed in a 90 °C bath for 14 h. After 14 h, the solvent was removed in vacuo, and the resulting yellow solid was washed with petroleum ether and collected on a sintered glass funnel as 68 mg (51% yield) of a white powder. ^{1}H NMR (300 MHz, CD_2Cl_2): δ 1.065 (s, 1H, Ta−N*H*Ph); 1.394 (s, 18H, C(C*H*$_3$)$_3$); 1.428 (s, 18H, C(C*H*$_3$)$_3$); 4.106 (s, 2H, Ta−N*H*$_2$Ph); 5.96 (d + t, 3H, aryl-*H*); 6.358 (d, 2H, aryl-*H*); 6.505 (t, 1H, aryl-*H*); 6.575 (d, 2H, aryl-*H*); 6.853 (t, 2H, aryl-*H*); 6.893 (t, 2H, aryl-*H*); 7.035 (t, 1H, aryl-*H*); 7.213 (t, 2H, aryl-*H*); 7.596 (s, 1H, aryl-*H*); 7.635 (s, 1H, aryl-*H*); 7.892 (d, 2H, 3,5-C_5NH_3); 8.038 (t, 1H, p-C_5NH_3). ^{13}C NMR (125 MHz, CD_2Cl_2): δ 29.87 (C(*C*H$_3$)$_3$); 31.71 (C(*C*H$_3$)$_3$); 34.62 (*C*(CH$_3$)$_3$); 35.38 (*C*(CH$_3$)$_3$); 118.47, 119.26, 119.43, 122.07, 123.51, 124.07, 124.31, 125.50, 126.68, 127.17, 127.47, 128.15, 129.59, 138.71, 139.29, 141.16, 141.34, 153.50, 115.83, 156.30, 159.73 (aryl). Anal. calcd for $C_{51}H_{61}N_4O_2Ta$: C, 64.96; H, 6.52; N, 5.94. Found: C, 66.26; H, 6.44; N, 5.96%.

(2,6-$(OC_6H_2$-$^tBu_2)_2C_5H_3N)Ta(NMe_2)_3$ (2). In an inert atmosphere glovebox, 2,6-$(HOC_6H_2$-$^tBu_2)_2C_5H_3N$ (200 mg, 0.4115 mmol, 1 equiv) and $Ta(NMe_2)_5$ (165 mg, 0.4115 mmol, 1 equiv) were mixed in a 20 mL vial with 2 mL of Et_2O. The reaction was stirred for 4 h, resulting in a mustard-colored precipitate and a darker yellow solution. After 4 h, the solvent and $HNMe_2$ were removed in vacuo, yielding 311 mg (95% yield) of **2** as a yellow solid. X-ray-quality crystals were obtained by the cooling of a saturated Et_2O solution of **3** to −30 °C overnight. ^{1}H NMR (300 MHz, C_6D_6): δ 1.429 (s, 18H, C(C*H*$_3$)$_3$); 1.749 (s, 18H, C(C*H*$_3$)$_3$); 2.975 (s, 12H, Ta-(N(C*H*$_3$)$_2$)$_2$); 3.741 (s, 6H, Ta−N(C*H*$_3$)$_2$) 7.078 (t, 1H, 4-C_5NH_3); 7.227 (d, 2H, 3,5-C_5NH_3); 7.520 (d, 2H, aryl-*H*); 7.637 (d, 2H, aryl-*H*). ^{13}C NMR (125 MHz, C_6D_6): δ 30.67 (C(*C*H$_3$)$_3$); 32.48 (C(*C*H$_3$)$_3$); 34.88 (*C*(CH$_3$)$_3$); 36.09 (*C*(CH$_3$)$_3$); 45.28 (N(*C*H$_3$)$_2$); 47.57 (N(*C*H$_3$)$_2$); 123.26, 123.99, 124.99, 127.52, 137.76, 138.57, 140.76, 155.14, 159.96 (aryl). Anal. calcd for $C_{39}H_{61}N_4O_2Ta$: C, 58.63; H, 7.70; N, 7.01. Found: C, 58.40; H, 7.10; N, 6.79%.

(2,6-$(OC_6H_2$-$^tBu_2)_2C_5H_3N)Ta(NMe_2)_2Cl$ (3). In an inert atmosphere glovebox, **2** (69 mg, 0.087 mmol, 1 equiv) was dissolved in 4 mL of C_6H_6, and 11 μL of TMSCl (0.087 mmol, 1 equiv) was syringed in. The reaction was sealed and stirred for 48 h. After the reaction was complete, volatile coproducts were removed in vacuo, quantitatively yielding **3** as a yellow solid. X-ray-quality crystals were grown from the slow evaporation of a saturated Et_2O solution of **3**. ^{1}H NMR (300 MHz, $C_6D_5CD_3$): δ 1.325 (s, 18H, C(C*H*$_3$)$_3$); 1.763 (s, 18H, C(C*H*$_3$)$_3$); 3.029 (s, 6H, N(C*H*$_3$)$_2$); 3.919 (s, 6H, N(C*H*$_3$)$_2$); 7.121 (t, 1H, 4-C_5NH_3); 7.338 (d, 2H, aryl-*H*); 7.477 (d, 2H, 3,5-C_5NH_3); 7.704 (d, 2H, aryl-*H*). ^{13}C NMR (125 MHz, C_6D_6): δ 31.06 (C(*C*H$_3$)$_3$); 32.19 (C(*C*H$_3$)$_3$); 34.99 (*C*(CH$_3$)$_3$); 36.09 (*C*(CH$_3$)$_3$); 47.59 (N(*C*H$_3$)$_2$); 49.45 (N(*C*H$_3$)$_2$); 123.65, 126.57, 128.95, 138.69, 139.29, 143.37, 154.62, 157.88 (aryl). Anal. calcd for $C_{37}H_{55}ClN_3O_2Ta$: C, 56.23; H, 7.02; N, 5.32. Found: C, 57.09; H, 6.33; N, 4.74%.

(2,6-$(OC_6H_2$-$^tBu_2)_2C_5H_3N)Ta(NPh)(HNMe_2)Cl$ (4). Complex **3** (11 mg, 0.014 mmol, 1 equiv) and aniline (1.3 μL, 0.014 mmol, 1 equiv) were mixed together in a J-Young NMR tube with 0.7 mL of C_6D_6. The vessel was sealed and heated to 90 °C in an oil bath. The reaction was monitored by ^{1}H NMR, and after 3 days at 90 °C, the reaction was complete, as confirmed by the disappearance of the Ta−NMe_2 peaks. The solvent and $HNMe_2$ was removed in vacuo, yielding **4** quantitatively. X-ray-quality crystals were grown from slow evaporation of a saturated solution of **4** in benzene. ^{1}H NMR (300 MHz, C_6D_6): δ 1.37 (s, 18H, C(C*H*$_3$)$_3$); 1.71 (s, 6H, N(C*H*$_3$)$_2$); 1.78 (s, 18H, C(C*H*$_3$)$_3$); 6.33 (d, 2H, aryl-*H*); 6.46 (t, 1H, aryl-*H*); 6.88 (t, 2H, aryl-*H*); 6.94 (t, 1H, 4-C_5NH_3); 7.25 (d, 2H, 3,5-C_5NH_3); 7.30 (d, 2H, aryl-*H*); 7.74 (d, 2H, aryl-*H*). ^{13}C NMR (125 MHz, C_6D_6): δ 30.8 (C(*C*H$_3$)$_3$); 32.3 (C(*C*H$_3$)$_3$); 34.9 (*C*(CH$_3$)$_3$); 36.0 (*C*(CH$_3$)$_3$); 38.5 (N(*C*H$_3$)$_2$); 123.3, 123.9, 125.2, 126.3, 127.2, 127.3, 127.8, 138.6, 139.3, 142.2, 156.4, 158.2, 159.5 (aryl).

(2,6-$(OC_6H_2$-$^tBu_2)_2C_5H_3N)Ta(NPh)(NH_2Ph)Cl$ (5). Complex 3 (12 mg, 0.0152 mmol, 1 equiv) and aniline (2.8 μL, 0.031 mmol, 2.1 equiv) were mixed together in a J-Young NMR tube with 0.7 mL of C_6D_6. The vessel was sealed and heated to 90 °C in an oil bath. The reaction was monitored by ^{1}H NMR, and after 3 days at 90 °C, the reaction was complete, as confirmed by the disappearance of the Ta−NMe_2 peaks. The solvent, excess aniline, and $HNMe_2$ were removed in vacuo, yielding **5** quantitatively. X-ray-quality crystals were grown from slow evaporation of a saturated solution of **5** in toluene. ^{1}H NMR (300 MHz, C_6D_6): δ 1.37 (s, 18H, C(C*H*$_3$)$_3$); 1.77 (s, 18H, C(C*H*$_3$)$_3$); 2.92 (br s, 2H, N*H*$_2$); 6.31 (2d, 4H, aryl-*H*); 6.46 (t, 1H, aryl-*H*); 6.69 (t, 1H, aryl-*H*); 6.88 (t, 2H, aryl-*H*); 6.98 (m, 3H, 4-C_5NH_3 + aryl-*H*); 7.25 (d, 2H, 3,5-C_5NH_3); 7.29 (d, 2H, aryl-*H*); 7.73 (d, 2H, aryl-*H*). ^{13}C NMR (125 MHz, C_6D_6): δ 30.9 (C(*C*H$_3$)$_3$); 32.2 (C(*C*H$_3$)$_3$); 34.9 (*C*(CH$_3$)$_3$); 36.1 (*C*(CH$_3$)$_3$); 123.3, 123.5, 125.2, 125.4, 126.3, 127.1, 127.2, 127.8, 129.6, 138.6, 139.1, 139.3, 142.2, 157.3, 158.2, 159.4 (aryl).

(2,6-$(OC_6H_2$-$^tBu_2)_2C_5H_3N)Ta(NMe_2)MeCl$ (6). (2,6-$(OC_6H_2$-$^tBu_2)_2C_5H_3N)TaCl_2Me$ (159 mg, 0.212 mmol, 1 equiv) was dissolved in 10 mL of C_6H_6 in an inert atmosphere glovebox, transferred to a 50 mL round-bottom flask equipped with a

(45) Frisch, M. J.; Trucks, G. W.; Schlegel, H. B.; Scuseria, G. E.; Robb, M. A.; Cheeseman, J. R.; Montgomery, J. A., Jr.; Vreven, T.; Kudin, K. N.; Burant, J. C.; Millam, J. M.; Iyengar, S. S.; Tomasi, J.; Barone, V.; Mennucci, B.; Cossi, M.; Scalmani, G.; Rega, N.; Petersson, G. A.; Nakatsuji, H.; Hada, M.; Ehara, M.; Toyota, K.; Fukuda, R.; Hasegawa, J.; Ishida, M.; Nakajima, T.; Honda, Y.; Kitao, O.; Nakai, H.; Klene, M.; Li, X.; Knox, J. E.; Hratchian, H. P.; Cross, J. B.; Bakken, V.; Adamo, C.; Jaramillo, J.; Gomperts, R.; Stratmann, R. E.; Yazyev, O.; Austin, A. J.; Cammi, R.; Pomelli, C.; Ochterski, J. W.; Ayala, P. Y.; Morokuma, K.; Voth, G. A.; Salvador, P.; Dannenberg, J. J.; Zakrzewski, V. G.; Dapprich, S.; Daniels, A. D.; Strain, M. C.; Farkas, O.; Malick, D. K.; Rabuck, A. D.; Raghavachari, K.; Foresman, J. B.; Ortiz, J. V.; Cui, Q.; Baboul, A. G.; Clifford, S.; Cioslowski, J.; Stefanov, B. B.; Liu, G.; Liashenko, A.; Piskorz, P.; Komaromi, I.; Martin, R. L.; Fox, D. J.; Keith, T.; Al-Laham, M. A.; Peng, C. Y.; Nanayakkara, A.; Challacombe, M.; Gill, P. M. W.; Johnson, B.; Chen, W.; Wong, M. W.; Gonzalez, C.; Pople, J. A.; *Gaussian 03*, revision C.02; Gaussian, Inc.: Wallingford, CT, 2004.
(46) Becke, A. D. *Phys. Rev. A: At., Mol., Opt. Phys.* **1988**, *38*, 3098–3100.
(47) Becke, A. D. *J. Chem. Phys.* **1988**, *88*, 1053–1062.
(48) Perdew, J. P. *Phys. Rev. B: Condens. Matter Mater. Phys.* **1986**, *33*, 8800–8802.
(49) Lee, C.; Yang, W.; Parr, R. G. *Phys. Rev. B: Condens. Matter Mater. Phys.* **1988**, *37*, 785.
(50) Miehlich, B.; Savin, A.; Stoll, H.; Preuss, H. *Chem. Phys. Lett.* **1989**, *157*, 200.
(51) Hay, P. J.; Wadt, W. R. *J. Chem. Phys.* **1985**, *82*, 270–283.
(52) Wadt, W. R.; Hay, P. J. *J. Chem. Phys.* **1985**, *82*, 284–298.
(53) Hay, P. J.; Wadt, W. R. *J. Chem. Phys.* **1985**, *82*, 299–310.

Table 2. Crystal and Refinement Data for Complexes **1**, **2**, and **3**

	1	**2**	**3**
empirical formula	$C_{51}H_{61}N_4O_2Ta \cdot 11/2(C_6H_6)$	$C_{39}H_{61}N_4O_2Ta$	$C_{37}H_{55}N_3O_2ClTa \cdot 0.75(C_4H_{10}O)$
fw	1060.15	798.87	845.83
T (K)	100(2)	100(2)	100(2)
a, Å	25.7250(8)	9.8149(5)	14.7164(6)
b, Å	17.8546(5)	29.0840(14)	18.3370(7)
c, Å	23.6141(7)	14.0826(6)	31.2188(13)
α, deg			
β, deg	105.9790(10)	104.357(3)	101.802(2)
γ, deg			
volume, Å^3	10427.1(5)	3894.4(3)	8246.4(6)
Z	8	4	8
cryst syst	monoclinic	monoclinic	monoclinic
space group	$C2/c$	$P2_1/c$	$P2_1/n$
d_{calc}, g/cm^3	1.351	1.363	1.363
θ range, deg	2.07 to 43.26	1.65 to 33.20	1.68 to 47.98
μ, mm^1	2.154	2.858	2.767
abs. correction	none	semi emp.	semi emp.
GOF	1.117	1.426	2.760
R_1,[a] wR_2[b] [$I > 2\sigma(I)$]	0.0299, 0.0520	0.0350, 0.0448	0.0731, 0.1059

[a] $R_1 = \sum||F_o| - |F_c||/\Sigma|F_o|$. [b] $wR_2 = [\sum[w(F_o^2 - F_c^2)^2]/\sum[w(F_o^2)^2]^{1/2}$.

Teflon needle valve, sealed, and degassed on a high-vacuum line. A total of 4.7 mmol of degassed $HNMe_2$ was then vac-transferred into the round-bottomed flask, and the reaction was thawed and stirred for 1 h at room temperature. The orange solution turned dark yellow with a white precipitate (H_2NMe_2Cl). After the reaction was complete, the reaction was filtered through a sintered glass funnel in an inert atmosphere glovebox, and the filtrate was dried in vacuo, yielding 148 mg (89.5%) of **6** as a yellow powder. ^{1}H NMR (300 MHz, $C_6D_5CD_3$): δ 1.319 (s, 18H, C(CH_3)$_3$); 1.659 (s, 3H, Ta-CH_3); 1.808 (s, 18H, C(CH_3)$_3$); 3.214 (s, 6H, N(CH_3)$_2$); 7.031 (t, 1H, 4-C_5NH_3); 7.290 (d, 2H, aryl-*H*); 7.375 (d, 2H, 3,5-C_5NH_3); 7.767 (d, 2H, aryl-*H*). ^{13}C NMR (125 MHz, $C_6D_5CD_3$):δ 31.10 (C(*C*H$_3$)$_3$); 32.10 (C(*C*H$_3$)$_3$); 35.05 (*C*(CH$_3$)$_3$); 36.03 (*C*(CH$_3$)$_3$); 48.69 (N(*C*H$_3$)$_2$); 48.90 (Ta-*C*H$_3$); 123.77, 126.86, 126.96, 128.95, 139.14, 139.27, 144.86, 152.77, 157.98 (aryl). Anal. calcd for $C_{36}H_{52}ClN_2O_2Ta$: C, 56.80; H, 6.89; N, 3.68. Found: C, 55.58; H, 6.08; N, 3.36%.

[(2,6-(OC$_6$H$_2$-^{t}Bu$_2$)$_2$C$_5$H$_3$N)Ta(OH)]$_2$(μ-O)$_2$ (7). In an NMR tube, (2,6-(OC$_6$H$_2$-^{t}Bu$_2$)$_2$C$_5$H$_3$N)TaMe$_3$ (7.7 mg, 0.011 mmol, 1 equiv) was dissolved in 1 mL of C_6D_6, and 4 equiv of H_2O were quantitatively gas-transferred onto the solution on a high vacuum line. The yellow solution immediately turned clear with a significant amount of white precipitate. The solvent was decanted off in an inert atmosphere glovebox and the product dried in vacuo; crystals were obtained from a saturated solution of the mixture of products in CH_2Cl_2.

Table 3. Crystal and Refinement Data for Complexes **4**, **6**, and **7**

	4	**6**	**7**
empirical formula	$C_{41}H_{55}N_3O_2ClTa$	$C_{36}H_{52}N_2O_2ClTa \cdot C_4H_{10}O$	$C_{66}H_{86}N_2O_8Ta_2 \cdot 4(CH_2Cl_2)$
fw	838.28	835.32	1736.97
T (K)	100(2)	100(2)	100(2)
a, Å	9.9628(5)	47.432(2)	16.0570(7)
b, Å	10.6118(5)	13.7447(7)	12.8407(6)
c, Å	18.9240(9)	12.4876(6)	18.4561(9)
α, deg	80.804(3)		
β, deg	89.355(3)	100.510(3)	103.542(3)
γ, deg	81.578(3)		
volume, Å^3	1953.54(16)	8004.5(7)	3699.5(3)
Z	2	8	2
cryst syst	triclinic	monoclinic	monoclinic
space group	P1	$C2/c$	$P2_1/c$
d_{calc}, g/cm^3	1.425	1.386	1.559
θ range, deg	1.97 to 35.14	1.54 to 27.85	1.95 to 51.56
μ, mm^1	2.919	2.850	3.297
abs. correction	none	none	semi emp.
GOF	1.281	1.678	1.629
R_1,[a] wR_2[b] [$I > 2\sigma$(I)]	0.0326, 0.0452	0.0358, 0.0563	0.0250, 0.0388

[a] $R_1 = \sum||F_o| - |F_c||/\sum|F_o|$. [b] $wR_2 = [\sum[w(F_o^2 - F_c^2)^2]/\sum[w(F_o^2)^2]^{1/2}$.

X-Ray Crystal Data: General Procedure. Crystals were removed quickly from a scintillation vial to a microscope slide coated with Paratone N oil. Samples were selected and mounted on a glass fiber with Paratone N oil. Data collection was carried out on a Bruker KAPPA APEX II diffractometer with a 0.71073 Å Mo Kα source. The structures were solved by direct methods. All non-hydrogen atoms were refined anisotropically. Some details regarding refined data and cell parameters are available in Tables 2 and 3. Selected bond distances and angles are supplied in the corresponding figures.

Acknowledgment. We thank Dr. Nilay Hazari (Caltech) for assistance with the DFT calculations. DFT calculations were carried out using the Molecular Graphics and Computation Facility, College of Chemistry, University of California, Berkeley, California, with equipment support from NSF grant CHE-0233882. This work has been supported by USDOE Office of Basic Energy Sciences (Grant No. DE-FG03-85ER13431). The Bruker KAPPA APEXII X-ray diffractometer was purchased via an NSF CRIF:MU award to the California Institute of Technology, CHE-0639094.

Supporting Information Available: Tables of bond lengths, angles, and anisotropic displacement parameters for the presented solid-state structures. Structural drawing of **5**, which due to its twinned nature cannot be refined anisotropically. X-ray crystallographic data files (CIF) of compounds **1**−**7**. This material is available free of charge via the Internet at http://pubs.acs.org.